Desalination and Water Treatment
www.deswater.com
doi: 10.1080/19443994.2014.980327

57 (2016) 3037–3047
February

Taylor & Francis
Taylor & Francis Group

Preparation and characterization of CTA/m-ZnO composite membrane for transport of Rhodamine B

Ilker Akin*, Mustafa Ersoz

Department of Chemistry, Selcuk University, Konya 42075, Turkey, Tel. +90 332 223 3897; Fax: +90 332 241 2499; emails: ilker0997@gmail.com (I. Akin), mersoz@selcuk.edu.tr (M. Ersoz)

Received 17 February 2014; Accepted 20 October 2014

ABSTRACT

Here, we report on the fabrication of modified-ZnO nanoparticles enhanced membrane and evaluation of its performance. Cellulose triacetate (CTA) membranes were manufactured by diffusion induced phase inversion in DCM and were blended with modified(m) ZnO nanoparticles. The CTA/m-ZnO and CTA/ZnO composite membranes were characterized by Fourier transform infrared spectroscopy, SEM, AFM techniques and contact angle measurements. After optimization of pH, the concentrations of carriers in the membrane, Rhodamine B and the stripping phase concentrations, transport efficiency reached to 98% at pH 12. The results showed that the fabricated membrane embedded with modified nanoparticles significantly improved membrane features.

Keywords: Nanoparticles; ZnO; CTA; Composite membrane; Rhodamine B

1. Introduction

Cellulose triacetate (CTA) has an excellent salt-rejecting capability and is noted for its strength, toughness, flexibility, and resistance to hydrolysis and biological attack. Successful attempts have been made using CTA in composite membranes, melt extruded hollow fibers, and Loeb-type blend membranes [1–3]. The limited solubility of CTA in common solvents has precluded its use as a high flux and high-rejection membrane [4]. The common modification methods to develop the CTA membranes can be summarized as: grafting, coating, and blending. Grafting includes formation of covalent bonding between hydrophilic monomers and CTA membranes via chemical, photochemical, radiation, or plasma initiation. The polymethylacrylate, AAc monomer, and polybutylacrylate are the most widely studied hydrophilic monomer in the surface modification of CTA membranes via grafting [5,6]. In coating, a thin layer of hydrophilic polymer can be coated on the surface of CTA membranes via contact and evaporation. Hydrophilic CTA membranes can be easily prepared by immersing membranes in polyamide solution [7]. Unlike grafting and coating methods which are post-fabrication modification, blending allows membrane modification during the fabrication phase. Blending is also considered to be the simplest method among these three methods which includes only physical mixing of CTA with hydrophilic polymers. In general, the hydrophobic polymer are used as a polysulfone (PSf). Besides blending with hydrophobic polymers, much attention has been recently given to blending of inorganic oxide nanoparticles [8]. Nanoparticles, having peerless physicochemical properties that vary from raw materials

*Corresponding author.

are of high interest in the manufacturing of membranes to obtain a high degree of check over membrane fouling and the ability to produce desired structures as well as functionalities [9–13]. Membrane fouling is the main problem and the costs associated with it. Nanoparticles may be a way to unzip this problem. The simplest method for preparing a composite membrane with intended nanoparticles is dispersion of the preformed nanoparticles in a suitable polymer matrix [13–21]. Composite membranes have attracted attention on nanoparticles, such as Pt, Pd, Au, Ag, FeO, CdS, Ag_2S, Fe_2O_3, Fe_3O_4, TiO_2, SiO_2, Al_2O_3, ZrO_2, carbon nanotubes, and bimetallics [13,21–25]. Mixing nanoparticles such as ZrO_2, SiO_2, and TiO_2 with PSf membranes have gained common attention due to the notable changes of membrane properties, such as permeability, selectivity, mechanical strength, thermal resistance, and flux decrease pattern [26]. Most researchers are more interested in blending cellulose acetate membranes with micron ZnO particles to increase membrane hydrophilicity for pervaporation [27,28]. Wang et al. have fabricated Al_2O_3/cellulose acetate (CA) and ZnO/CA hybrid membranes. They found that the maximum flux of a hybrid membrane blended with nano Al_2O_3 and nano-ZnO improved to 96.5% and 111.1%, respectively, compared to that of a CA membrane. To the best of our knowledge, few reports about the filtration and antifouling properties of ZnO/PES hybrid membranes have been reported. These materials exhibit excellent permeability, selectivity, and stability in water and waste water applications. Dyes are widely used in various industries, such as plastics, textiles, paper, cosmetics, and leather, for coloring their final products. Color is the first contaminant to be recognized in wastewater. In recent years, several physicochemical decolorization processes have been developed, such as membrane separation. A number of different techniques are available in preparing composite membranes such as: phase inversion, sol–gel techniques, thin-film deposition, coating (layer-by-layer coatings, interfacial polymerization, dip-coating), etc. Different from these techniques, Mauter et al. have found a novel pathway for the fabrication of reactive membranes via post-synthesis grafting of nanoparticles to the membrane surface. This novel technique is used for covalently or ionically tethering antimicrobial nanoparticles to the surface of UF membranes [29]. In this study, CTA/ZnO and CTA/m-ZnO composite membranes were prepared by a phase inversion method and their properties including chemical composition, membrane morphology, and hydrophilicity were characterized by Fourier transform infrared spectroscopy (FT-IR), scanning electron microscopy (SEM), atomic force microscopy (AFM), and contact angle measurement. In addition, the fabricated membranes were employed to perform dye transport experiments with aqueous solutions of Rhodamine B (RB).

2. Experimental section

2.1. Materials

Zinc chloride ($ZnCl_2$), urea (CON_2H_4), ammonium hydroxide (NH_4OH), ethanol (CH_3CH_2OH), dichloromethane (CH_2Cl_2), 3-(aminopropyl)triethoxysilane (APTES), and CTA were purchased from Aldrich Chemical Co. RB was purchased from Merck. All the chemicals were of reagent grade and used without further purification. Distilled water was used throughout the study.

2.2. Synthesis of ZnO nanoparticles

ZnO nanoparticles were synthesized according to the literature [30] by adapting known synthetic procedures, respectively. $ZnCl_2$ (1.36 g) and urea (2.40 g) were dissolved in distilled water (100.0 ml) with a constant stirring for 30 min at room temperature and pH was adjusted to 10.2 by drop wise addition of NH_4OH solution. The resultant solutions were then transferred into a Teflon lines autoclave and heated up to 180°C for 9 h. White precipitates were obtained after cooling the reaction mixture at room temperature. The precipitates were washed with water and ethanol for several times and dried at room temperature. The resulting white powders were calcined at 400°C for 5 h.

2.3. Surface functionalization of ZnO nanoparticles

ZnO nanoparticles were dried at 120°C in an oven for 24 h to remove the adsorbed water. The dried ZnO nanoparticles (0.6 g) were ultrasonicated for 30 min in 30 mL of absolute ethanol and then, as shown in Fig. 1, 0.12 mL of 3-(aminopropyl)triethoxysilane(APTES) was added to the dispersed solution; then, the mixture was dispersed for 30 min through an ice–water ultrasonic bath. Finally, the suspension was filtered and washed with ethanol to remove unreacted APTES. The solid was dried at 60°C for more than 24 h [31].

2.4. Preparation of membrane

Firstly, m-ZnO nanoparticles were dried at 120°C in an oven for 24 h to remove the adsorbed water. CTA membranes blended with m-ZnO nanoparticles

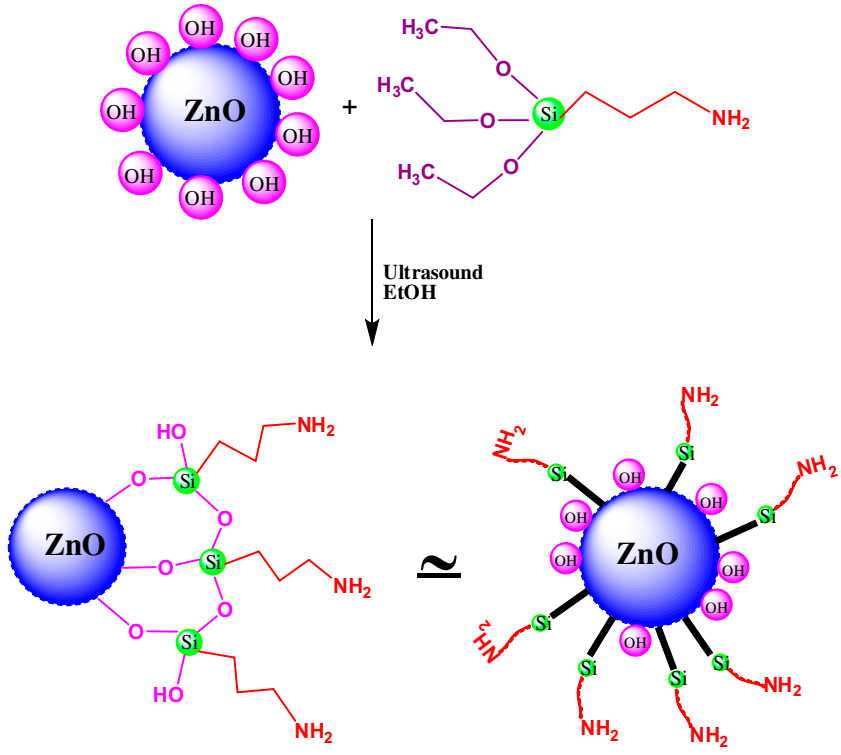

Fig. 1. Surface modification of ZnO nanoparticles with 3-(aminopropyl)triethoxysilane (APTES).

were prepared using phase inversion method. The casting solution was prepared by distributing m-ZnO nanoparticles in dichloromethane (DCM). CTA (200 mg) was dissolved in 20 mL of DCM at room temperature. 0.3 mL of 2-NPOE in 5 mL of dichloromethane was added. After vigorous stirring, a solution containing the m-ZnO nanoparticles were added and the solution was stirred for 30 min to obtain a homogeneous solution. Dichloromethane was allowed to evaporate overnight, and the resulting membrane was separated from glass plate by immersion into cold water after the membrane was soaked in distilled water for 1 h [32,33]. The membrane preparation is given schematically in Fig. 2.

2.5. Surface characterization

In order to characterize the composite membranes, FT-IR, AFM techniques, and contact angle measurements were used. AFM images were obtained by Solver Pro AFM from NT-MDT (Russia). The speed of scanning was 2 kHz. Tapping mode of AFM in air was used to investigate the surface morphology of membranes. The structure of membrane samples was

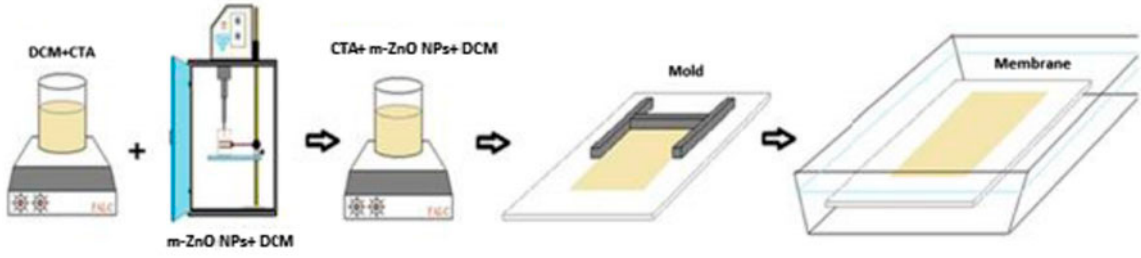

Fig. 2. Preparation of membrane.

examined using SEM EVO-LS 10 (Carl Zeiss, Germany). FT-IR spectrums were acquired using ATR FT-IR spectrometer (Perkin-Elmer 100 FT-IR). Measurements were taken in wave number from 400 to 4,000 cm^{-1}. The sessile drop method was used to measure the contact angle of the prepared membranes [34,35]. A 4 μL droplet of distilled water was placed on the membrane surface by means of a 0.10 mL syringe, and contact angle was measured by a horizontal beam comparator (KSV CAM 200). A magnified image of the droplet was recorded by a digital camera. Static contact angles were determined from these images with calculation software. The contact angle measurement was taken as the mean value of three different points on each membrane.

2.6. Transport experiments

The transport experiments were carried out using a cell consisting of two detachable Teflon chambers. The PIM was placed between the chambers and the chambers were tightened with screws. The silicone rubber seals were used to prevent any leakage from the chambers. Equal volumes (40 mL) of the feed and stripping phases were placed in the respective chambers of the transport cell. In each experiment, the stirring rates of both phases were equal and constant at 350 rpm throughout the experiment. All experiments were performed at 25 ± 1°C and effective membrane area was 7.0 cm^2 [33].

The studied experimental parameters were RB concentration of the feed phase 0.005–0.1 (%w/w), initial pH (8.0–13.0) and, stripping phase (HCl) concentration of (0.1–3.0 M), carrier concentration of the casting solution (0.1–3.0%), transport time, and stripping speed(150–400 rpm).

The transport of RB was also defined according to Eq. (1);

$$\text{Transport } (\%) = 100 \times \left(\frac{C_s}{C_0}\right) \quad (1)$$

where C_s is the concentration of RB in the stripping phase at time t and C_0 is the initial concentration of RB in the feed phase.

In order to determine the concentration of RB, samples of 1 mL were periodically withdrawn from the feed and stripping phases over transport time, and analyzed by UV spectrophotometer (Shimadzu UV-1800, JAPAN).

Table 1
Peak values and the corresponding radical in membranes

Membrane	Peak value (cm^{-1})	Corresponding radical
CTA	3,480	O–H
	2,950	C–H
	1,740	C=O
	1,350	C–H (deformation of CH_3)
	1,210 and 1,030	C–O
ZnO	504	Zn–O
	3,448 and 1,635	O–H
CTA/m-ZnO	Same bands in addition to	
	2,975	H–C–NH_2
	2,850	C–H
	817	Si–O–CH_3
	954	Si–O–Zn

3. Results and discussion

3.1. Characterization

FT-IR spectra of CTA, ZnO nanoparticles, and CTA/m-ZnO are shown in Table 1. The appearance of a band at 504 cm^{-1} in the FT-IR spectra confirms the synthesis of ZnO, because it is the characteristic absorption band for the Zn–O stretching vibration [36]. In the pure ZnO nanoparticles peak values (Table 1), a broad absorption peaks centered at around 3,448 and 1,635 cm^{-1} are caused by the O–H stretching of the absorbed water molecules and carbon dioxide, because the nanocrystalline materials exhibit a high surface-to-volume ratio. A very small band originated at 882 cm^{-1} are probably due to the carbonate moieties which are generally observed when FT-IR samples are measured in air [37]. All these characteristic peaks suggesting the formation of ZnO nanoparticles. The IR spectra of the CTA exhibit weak band at 2,930 cm^{-1} which are attributed to the stretching modes of aliphatic C–H groups. The obtained results show the absorption band located around 1,740 cm^{-1}, which is attributed to stretching vibration of the carbonyl group. In addition, the absorption band at 1,370 cm^{-1} is due to CH deformation of CH_3. Two absorption bands at 1,030 and 1,210 cm^{-1} attributed to C–O stretching mode are also observed. In modified ZnO nanoparticles well-rounded membranes peak values, the existence of characteristic peaks of APTES, indicate the presence of coupling agent after functionalization. The peaks in the regions of 2,850 and 2,954 cm^{-1} correspond to the CH_2 and CH_3 groups of APTES. The disappearance of the peak at 817 cm^{-1} is attributed to

Si–O–CH_3, and the presence of a new peak at 954 cm^{-1} confirms the formation of Si–O–Zn bonds [29,31,38]. All these facts indicate that the silane molecules have been successfully grafted onto the surface of ZnO nanoparticles.

Membrane surfaces were investigated with SEM. The influence of the addition of ZnO and m-ZnO nanoparticles to the membrane surface is shown in Fig. 3. The SEM images of the CTA membrane surface before addition of ZnO nanoparticles were similar to those of the same membranes after embedding ZnO nanoparticles. However, further increase in added nanoparticles to 0.5 wt% promoted the formation of clusters or aggregates of ZnO on the membrane surface significantly. Also, the addition of m-ZnO increased of clusters and m-ZnO further aggregates formation on the membrane surface. Similar results were observed by Balta et al. [39].

The AFM was used to image the surface of CTA/ZnO and CTA/m-ZnO composite membranes. Fig. 4 shows the AFM images of composite membranes, respectively, in three-dimensional form with format of 10 μm × 10 μm. As can be seen in Fig. 4, the CTA/ZnO membrane is non-porous and only imperceptibly wrinkled with regard to different speed of the solvent vaporization. On the other hand, CTA/m-ZnO composite membrane is observed to has a smooth surface. As stated by Oh et al., although the overall surfaces remain unchanged, a partial contradistinction in the surfaces of the APTES-modified membranes was observed (the surface becomes comparatively smoother). These phenomena may be explained by self-polymerization of APTES. APTES has three ethoxy groups, which can transfer each other in the presence of protic solvent, which moves as a catalyst, instead of reacting with a hydroxyl group on the membrane surface. As a result,

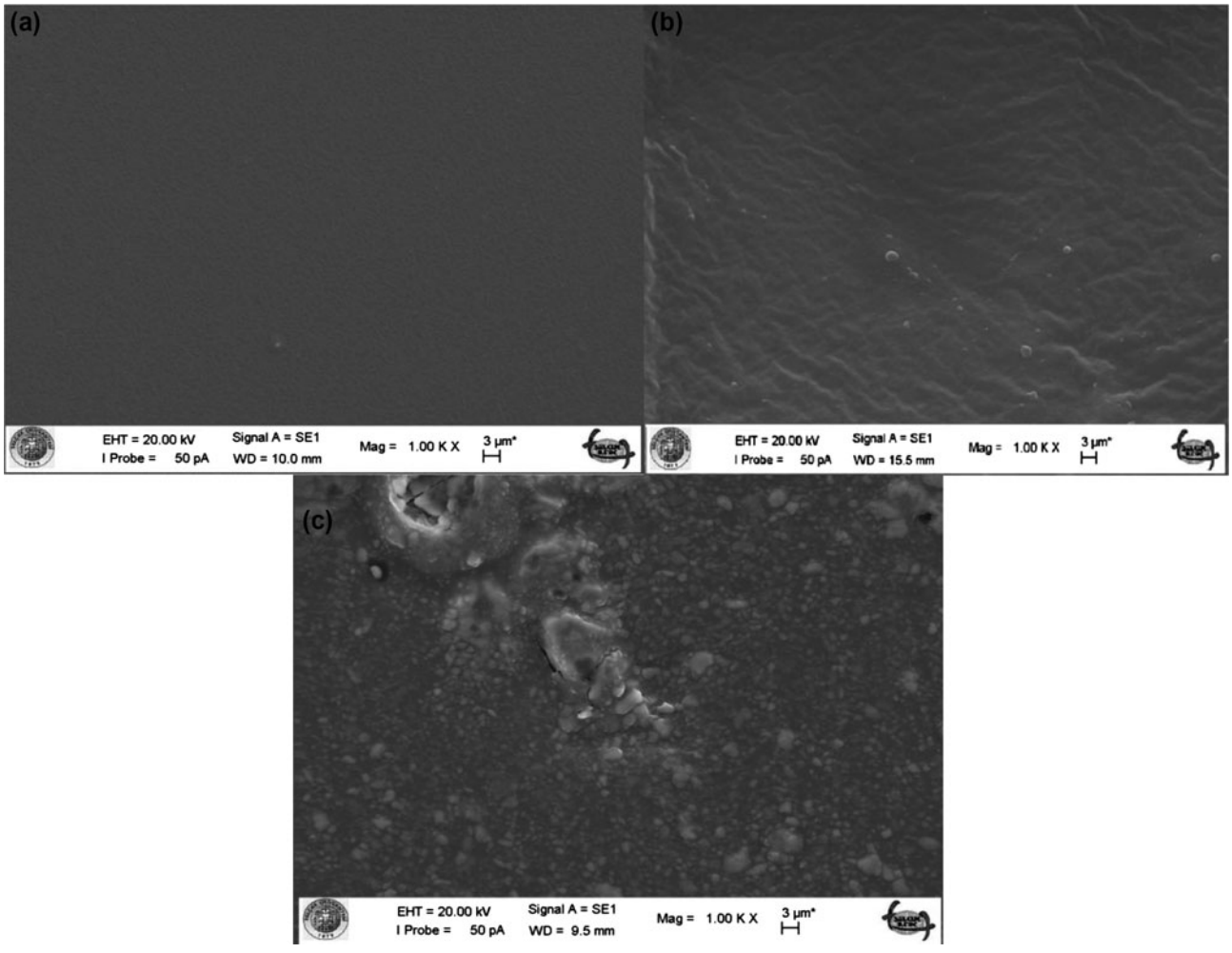

Fig. 3. SEM images of the surface of the synthesized membranes; CTA membrane (a), CTA/ZnO membranes (b), and CTA/m-ZnO nanoparticles composite membranes (c).

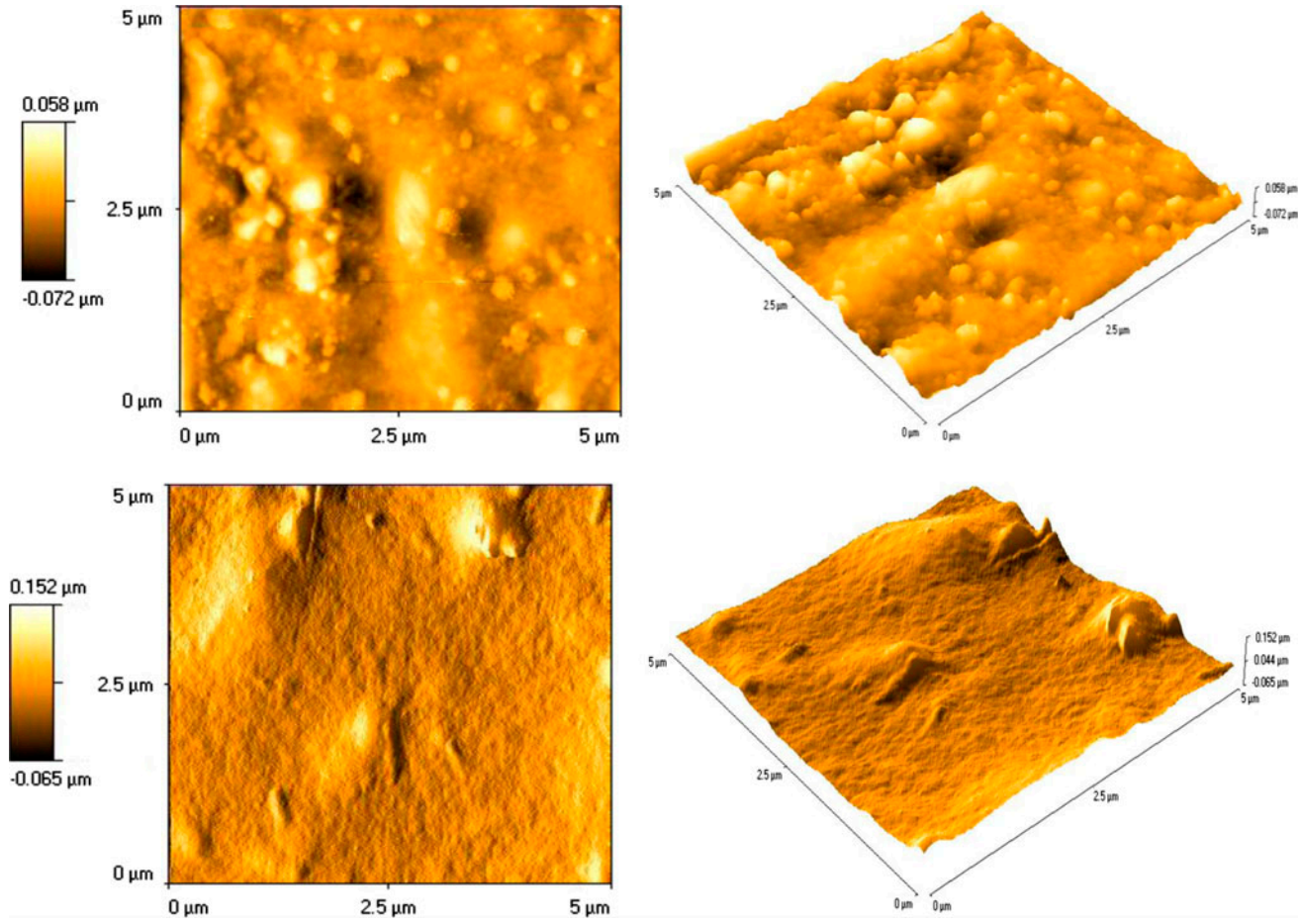

Fig. 4. AFM images of composite membranes; CTA/ZnO membrane and CTA/m-ZnO membrane, respectively.

some APTES molecules polymerize, which can cause the membrane surface to be smoother [40]. The roughnesses (*Ra*) for CTA/ZnO and CTA/m-ZnO were found to be 25.20 and 11.90 nm. The roughnesses values of CTA/m-ZnO with respect to CTA/ZnO are indicative of a smoother surface.

Contact angle measurement is used to investigate the hydrophilicity of the material surfaces [20]. Fig. 5(a)–(c) shows the contact images taken at room temperature for CTA membrane, CTA/ZnO and CTA/m-ZnO composite membranes were found to be 50° ± 1°, 53° ± 2°, and 67° ± 1°, respectively (n = 3). The reason why CTA membrane has lower contact angle than CTA/ZnO and CTA/m-ZnO membranes are due to the inclusion of the ZnO and m-ZnO nanoparticles in the CTA support. The increase in the contact angle values means a decrease in the wettability of membrane surface. The obtained images of the membranes are shown in Fig. 6.

4. Transport experiments

4.1. Effect of initial pH of feed phase

In order to investigate the effect of initial pH of the feed phase on the transport of Rhodamin B (RB), the experiments were performed at initial pH of 8.0, 9.0, 10.0, 11.0, 12.0, and 13.0. The results are presented in Fig. 7. A pH deviation of ±0.2 was observed for each pH measurement. It was found that the transport of RB increased with initial pH up to 12.0. The optimum value in the present study appears to be about pH 12 in which a high degree of RB transport is achievable. As shown in the results, CTA/m-ZnO membrane is better than CTA/ZnO membrane in the transport of RB and the other parameters were used in CTA/m-ZnO membrane for the transport of Rhodamine. Similar results were observed by Elumalai and Muthuraman [41]. Transport apparatus compartment stripping phase, the dye–m-ZnO complex reacts with HCl in the membrane stripping interface and

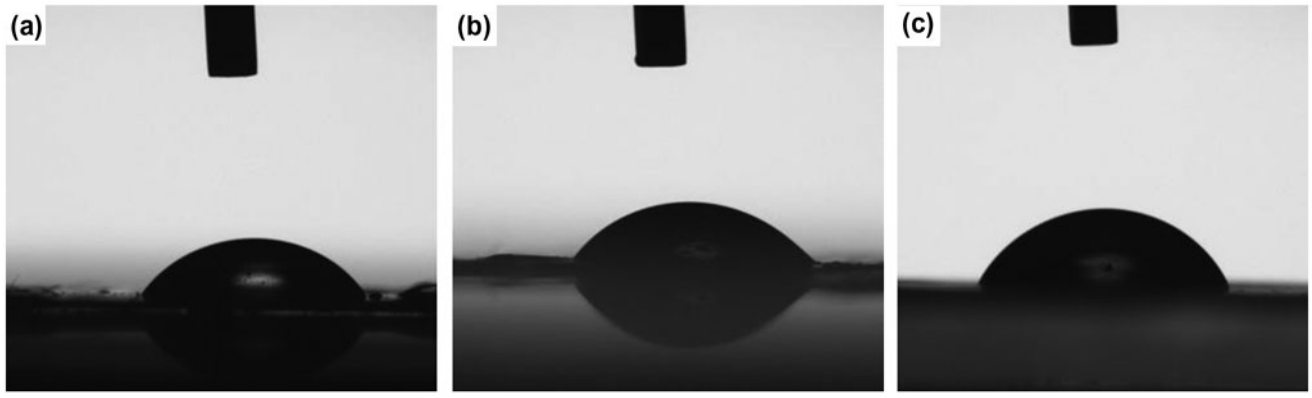

Fig. 5. Contact images of CTA membrane (a), CTA/ZnO membrane (b), and CTA/m-ZnO membrane (c).

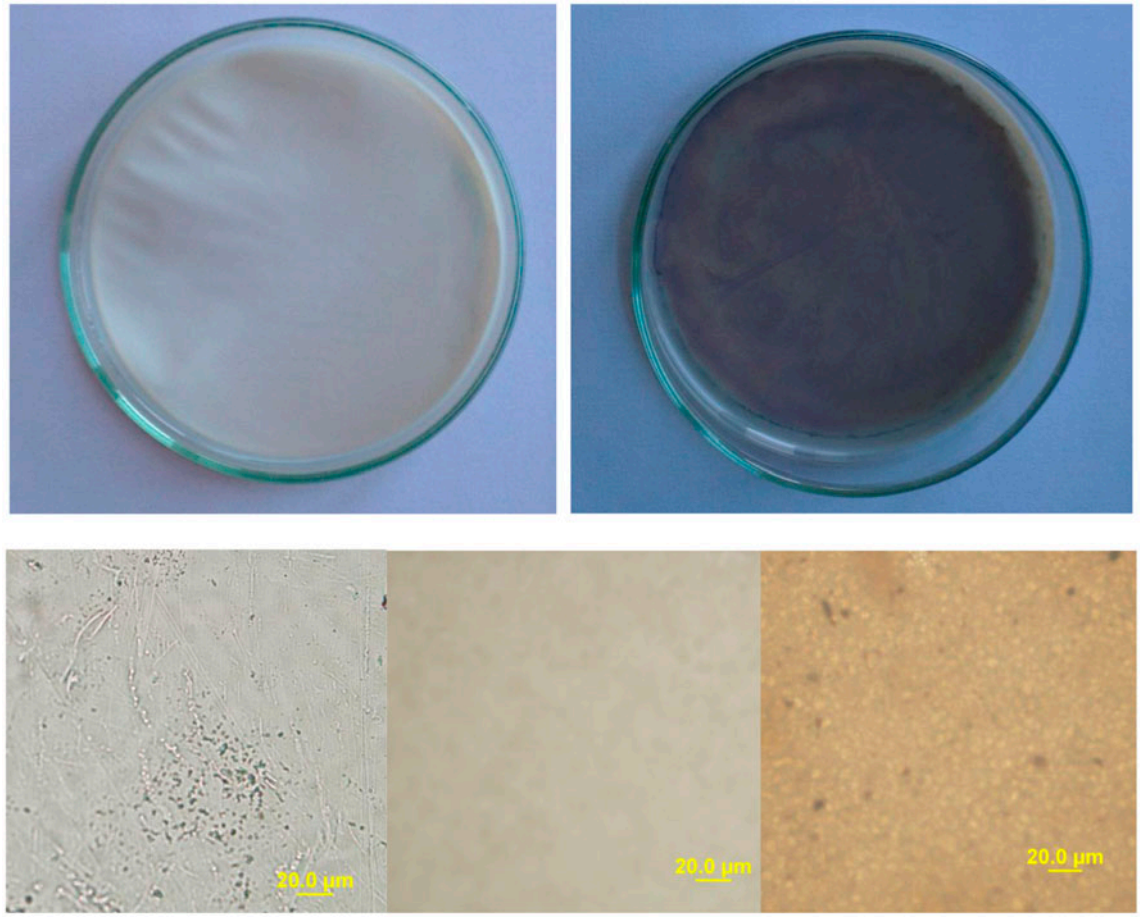

Fig. 6. Images and light microscope images of the membrane surface; CTA membrane, CTA/ZnO membranes, and CTA/m-ZnO nanoparticles composite membranes, respectively.

then dye diffuses into the stripping phase. The proposed mechanism is shown in Fig. 8.

4.2. Effect of stripping phase concentration

The dependence of the transport of RB with the hydrochloric acid concentration is shown in Fig. 9. When the HCl concentration increases, the transport of RB also increases. The concentration of HCl was varied from 0.1 to 3.0 M. In this case, the ionic strength of the feed phase was also maintained from 0.1 to 3.0 M using NaCl. The presence of HCl in the stripping phase helps the transport of dye by converting the dye hydrophilic moiety. The transport of dye linearly increased with HCl acid concentration until 1.0 M. It was observed that the transport of RB decreases in higher concentration of hydrochloric acid, due to the mass action effect of chloride ions. A similar effect was observed for the extraction of these metals with Kelex 100 [42].

4.3. Effect of RB concentration of feed phase

In order to assess the influence of the RB concentration on its transport through the composite membrane, the transport experiments were carried out at four different concentrations in the range of % 0.005–% 0.1. The results are shown in Fig. 10. For a transfer time of 8 h, it is observed that the transfer percentage decreased from 98 to 57% upon increasing concentration of RB from % 0.005 to % 0.1 in the feed phase. Similar result was also reported in Ref. [43]. The influence of the RB concentration on the transport is also evaluated using flux values, which are defined according to Eq. (2) [44].

$$J = P \times C_i \tag{2}$$

The flux values were in the range of $(0.90) \times 10^{-8}$–$(5.49) \times 10^{-8}$ mol ($cm^{-2}s^{-1}$) for different concentration

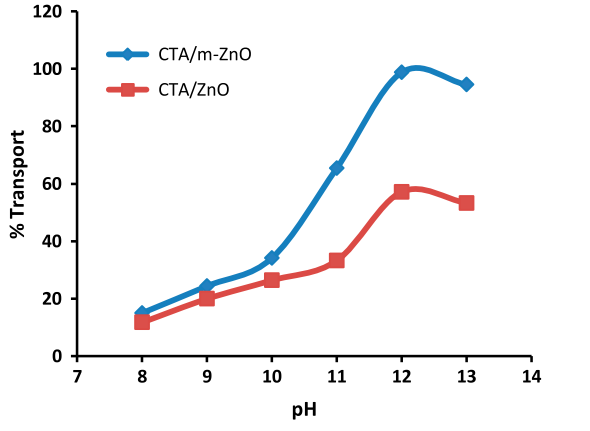

Fig. 7. Effect of initial pH of the feed phase on the transport of RB through the composite membranes. (Feed phase: 50 mg L^{-1} RB, stripping phase: 1.0 M HCl.)

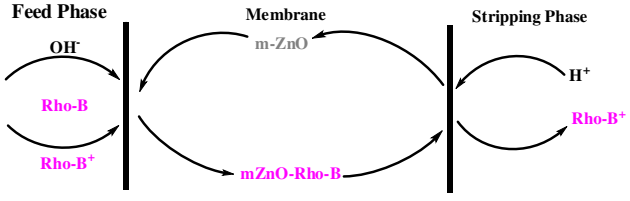

Fig. 8. Schematic description of transport of dye through composite membrane.

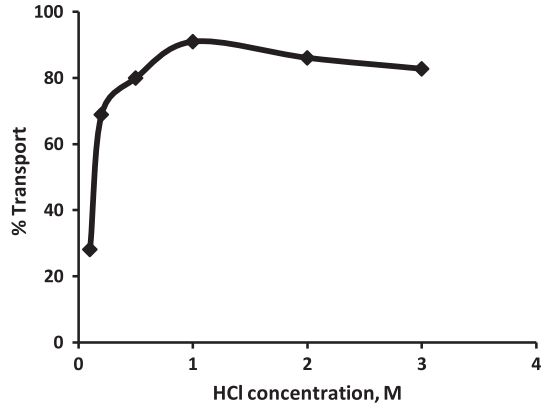

Fig. 9. Effect of stripping phase concentration on the transport of RB. (Feed phase: 50 mg L^{-1} RB, initial pH of the feed phase: 12.0 ± 0.2.)

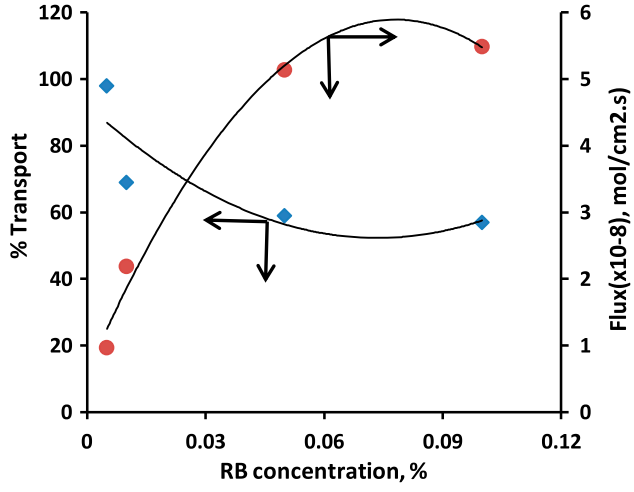

Fig. 10. Effect of RB concentration of the feed phase on the transport (initial pH of the feed phase: 12.0±0.1, stripping phase: 1 M HCl).

of RB from % 0.005 to % 0.1. The obtained result is in accordance with the expected trend, because according to Eq. (2) higher concentration results in a higher flux and increasing the concentration of RB in the feed phase decreased the transport percentage.

4.4. Effect of carrier concentration

The carrier concentration of membrane has a significant effect on dye transport across the membrane. The effect of m-ZnO amount on the transport of RB was investigated under four different carrier concentrations: 0.1, 0.5, 1.0, and 3.0%. The result showed that the transport of RB increased with increasing the amount of carrier up to 1.0% (Fig. 11). This may be explained by considering the formation of RB–m-ZnO complex at the feed/membrane interface. The RB/m-ZnO complex formation increases with increasing carrier concentration and the membrane becomes saturated in RB/m-ZnO complex at higher m-ZnO concentration. In other words, this result may be due to a steric hindrance effect. The literature also shows similar result with the different carriers [45,46].

4.5. Effect of transport time and stirring speed

A series of experiments were performed to optimize the transport time at initial concentration of 50 mg L^{-1} by composite membrane. The results obtained are shown in Fig. 12.

Fig. 13 shows the influence of stirring speed on the transport of the RB. The result indicates that transport efficiency increase in increasing the speed and the optimum transport efficiency was obtained at 350 rpm. For the speed faster than 350 rpm, the decrease in permeability is the consequence of the turbulence caused by stirring. Similar results were also reported in Ref. [47,48]. Further research studies were done at 350 rpm.

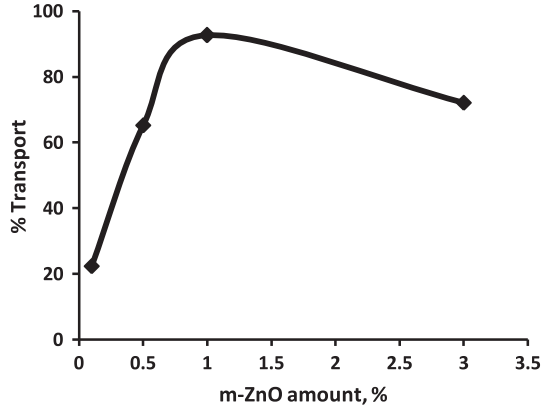

Fig. 11. Effect of m-ZnO amount on the transport of RB through the composite membrane. (Feed phase: 50 mg L^{-1} RB, initial pH of the feed phase: 12.0 ± 0.2, stripping phase: 1 M HCl.)

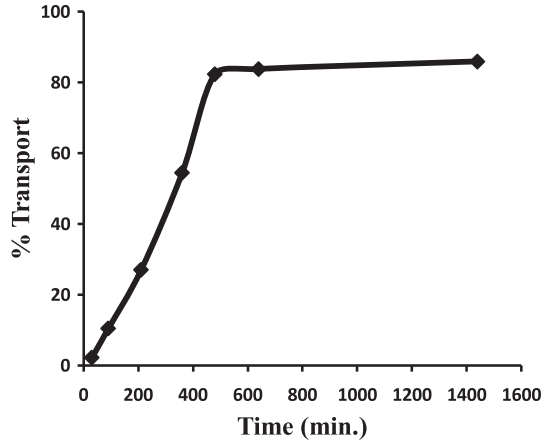

Fig. 12. Effect of contact time on the transport of RB through the CTA/m-ZnO composite membrane. (Feed phase: 50 mg L^{-1} RB, stripping phase: 1.0 M HCl.)

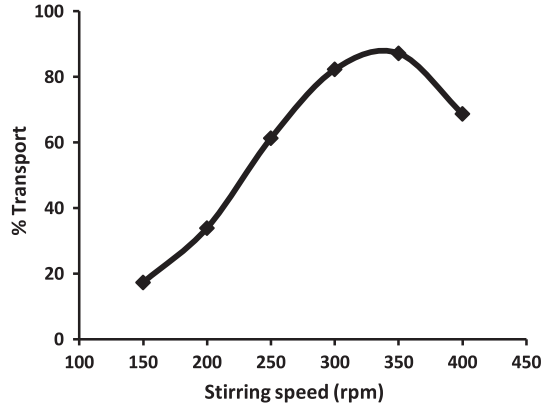

Fig. 13. Effect of stirring speed on the transport of RB through the CTA/m-ZnO composite membrane. (Feed phase: 50 mg L^{-1} RB, stripping phase: 1.0 M HCl.)

5. Conclusions

In this study, the transport of RB through a novel composite membrane a well-rounded modified nano-ZnO was investigated. First, the prepared membrane was characterized by FT-IR, SEM and AFM techniques, and contact angle measurements. Then, the transport experiments were carried out. The obtained results can be concluded as follows:

(1) The transport of RB through the composite membrane was influenced by a number of variables, including initial pH and RB concentration of the feed phase, concentration of the stripping phase, transport time and stirring speed, and m-ZnO nanoparticle concentration of the composite membrane.
(2) The results from the characterization studies corroborated that m-ZnO was successfully introduced into the CTA polymeric matrix. Thus, the preparation of the composite membrane was achieved.
(3) The maximum transport of RB was obtained when the following experimental conditions were employed: initial pH of feed phase 12.0 ± 0.1, membrane prepared with 1.0% m-ZnO nanoparticles, stirring speed 350 rpm, transport time 8 h, and stripping phase of 1 M HCl. In addition, increasing the concentration of RB in the feed phase decreased the transport percentage.
(4) The resulting membrane of the chemical activation has really increased the capacity of retention of this natural material. It may be applied for recovery of dyes from textile effluent in textile industry.

Acknowledgments

We thank the scientific research projects foundation of Selcuk University (SUBAP-Grant Number 2012-12101026) for financial support of this work produced from a part of I. Akin's PhD Thesis.

References

[1] K. Furukawa, M. Sekino, H. Matsumoto, K. Hamada, T. Ukai, H. Matshui, Permeability properties of CTA hollow-fiber membranes for one-pass seawater desalination, in: A.F. Turbak (Ed.), Synthetic Membranes, vol. 1, Paper No. 15, IIT Rayonier Inc., Lincoln, 1981, pp. 223–234.
[2] E.L. Dance, Development of cellulose triacetate hollow-fiber reverse osmosis modules or brackish water desalination, OSW, Res. Develop. Progr. Rept., No. 763, 1971.
[3] W.M. King, P.A. Cantor, L.W. Schoellenbach, C.R. Cannon, High retention reverse osmosis desalination membranes from cellulose acetate, in A.F. Turbak (Ed.), Appl. Polym. Symposia 13 (1970) 17, International Scientific Publications, New York, NY.
[4] S.V. Joshi, A.V. Rao, Cellulose triacetate membranes for seawater desalination, Desalination 51 (1984) 307–312.
[5] R.O. Mazzei, E. Smolko, A. Torres, D. Tadey, C. Rocco, L. Gizzi, S. Strangis, Radiation grafting studies of acrylic acid onto cellulose triacetate membranes, Radiat. Phys. Chem. 64 (2002) 149–160.
[6] R.M. Asimova, V.N. Yegovora, P.V. Kozlov, R.M. Livshits, Z.A. Rogovin Sb. Tsellulosa i ee proizvodnye (Collected Papers. Cellulose and its Derivatives), p. 100. Izd. Akad. Nauk SSSR, 1963.
[7] I.L. Alsvik, K.R. Zodrow, M. Elimelech, M.B. Hägg, Polyamide formation on a cellulose triacetate support for osmotic membranes: Effect of linking molecules on membrane performance, Desalination 312 (2013) 2–9.
[8] C.P. Leo, W.P. Cathie Lee, A.L. Ahmad, A.W. Mohammad, Polysulfone membranes blended with ZnO nanoparticles for reducing fouling by oleic acid, Sep. Purif. Technol. 89 (2012) 51–56.
[9] J.F. Li, Z.L. Xu, H. Yang, L.Y. Yu, M. Liu, Effect of TiO_2 nanoparticles on the surface morphology and performance of microporous PES membrane. Appl. Surf. Sci. 255 (2009) 4725–4732.
[10] M.M. Cortalezzi, J. Rose, A.R. Barron, M.R. Wiesner, Characteristics of ultrafiltration ceramic membranes derived from alumoxane nanoparticles, J. Membr. Sci. 205 (2002) 33–43.
[11] M.M. Cortalezzi, J. Rose, G.F. Wells, J.Y. Bottero, A.R. Barron, M.R. Wiesner, Ceramic membranes derived from ferroxane nanoparticles: A new route for the fabrication of iron oxide ultrafiltration membranes, J. Membr. Sci. 227 (2003) 207–217.
[12] I. Soroko, A. Livingston, Impact of TiO_2 nanoparticles on morphology and performance of crosslinked polyimide organic solvent nanofiltration (OSN) membranes, J. Membr. Sci. 343 (2009) 189–198.
[13] J. Kim, B. Van der Bruggen, The use of nanoparticles in polymeric and ceramic membrane structures: Review of manufacturing procedures and performance improvement for water treatment, Environ. Pollut. 158 (2010) 2335–2349.
[14] Y.N. Yang, H.X. Zhang, P. Wang, Q.Z. Zheng, J. Li, Effect of TiO_2 nanoparticles on the surface morphology and performance of microporous PES membrane, J. Membr. Sci. 288 (2007) 231–238.
[15] L. Yan, Y.S. Li, C.B. Xiang, Preparation of poly(vinylidene fluoride) (PVDF) ultrafiltration membrane modified by nano-sized alumina (Al_2O_3) and its antifouling research, Polymer 46 (2005) 7701–7706.
[16] X.C. Cao, J. Ma, X.H. Shi, Z.J. Ren, Effect of TiO_2 nanoparticle size on the performance of PVDF membrane, Appl. Surf. Sci. 253 (2006) 2003–2010.
[17] L. Yan, Y.S. Li, C.B. Xıang, S. Xıanda, Effect of nano-sized $Al2O_3$-particle addition on PVDF ultrafiltration membrane performance, J. Membr. Sci. 276 (2006) 162.
[18] P. Jian, H. Yahui, W. Yang, L. Linlin, Preparation of polysulfone–Fe_3O_4 composite ultrafiltration membrane and its behavior in magnetic field, J. Membr. Sci. 284 (2006) 9–16.
[19] Y.N. Yang, P. Wang, Preparation and characterizations of a new PS/TiO_2 hybrid membranes by sol–gel process, Polymer 47 (2006) 2683–2688.
[20] C.M. Wu, T.W. Xu, W.H. Yang, Fundamental studies of a new hybrid (inorganic–organic) positively charged membrane: Membrane preparation and characterizations, J. Membr. Sci. 216 (2003) 269–278.
[21] E.S. Smotkin, R.M. Brown Jr., L.K. Rabenberg, K. Salomon, A.J. Bard, A. Campion, M.A. Fox, T.E.

Mallouk, S.E. Webber, J.M. White, Ultrasmall particles of cadmium selenide and cadmium sulfide formed in Nafion by an ion-dilution technique, J. Phys. Chem. 94 (1990) 7543–7549.
[22] H.W. Rollins, F. Lin, J. Johnson, J.-J. Ma, J.-T. Liu, M.-H. Tu, D.D. DesMarteau, Y.-P. Sun, Nanoscale cavities for nanoparticles in perfluorinated ionomer membranes, Langmuir 16 (2000) 8031–8036.
[23] P. Liu, J. Bandara, Y. Lin, D. Elgin, L.F. Allard, Y.-P. Sun, Formation of nanocrystalline titanium dioxide in perfluorinated ionomer membrane, Langmuir 18 (2002) 10389–10401.
[24] Y.-P. Sun, P. Atorngitjawat, Y. Lin, Nanoscale cavities in ionomer membrane for the formation of nanoparticles, J. Membr. Sci. 245 (2004) 211–217.
[25] N.H. Jalani, K. Dunn, R. Datta, Synthesis and characterization of Nafion®-MO_2 (M = Zr, Si, Ti) nanocomposite membranes for higher temperature PEM fuel cells, Electrochim. Acta 51 (2005) 553–560.
[26] R.A. Alvarez-Puebla, G.-A. Nazri, R.F. Aroca, Fabrication of stable bimetallic nanostructures on Nafion membranes for optical applications, J. Mater. Chem. 16 (2006) 2921–2924.
[27] Y. Wang, L. Yang, G. Luo, Y. Dai, Preparation of cellulose acetate membrane filled with metal oxide particles for the pervaporation separation of methanol/methyl tert-butyl ether mixtures, Chem. Eng. J. 146 (2009) 6–10.
[28] M. Ali, M. Zafar, T. Jamil, M.T.Z. Butt, Influence of glycol additives on the structure and performance of cellulose acetate/zinc oxide blend membranes, Desalination 270 (2011) 98–104.
[29] M.S. Mauter, Y. Wang, K.C. Okemgbo, C.O. Osuji, E.P. Giannelis, M. Elimelech, Antifouling ultrafiltration membranes via post-fabrication grafting of biocidal nanomaterials, ACS Appl. Mater. Interfaces 3 (2011) 2861–2868.
[30] M. Faisal, S.B. Khan, M.M. Rahman, A. Jamal, M.M. Abdullah, Fabrication of ZnO nanoparticles based sensitive methanol sensor and efficient photocatalyst, Appl. Surf. Sci. 258 (2012) 7515–7522.
[31] A. Abdolmaleki, S. Mallakpour, S. Borandeh, Preparation, characterization and surface morphology of novel optically active poly(ester-amide)/functionalized ZnO bionanocomposites via ultrasonication assisted process, Appl. Surf. Sci. 257 (2011) 6725–6733.
[32] O. Kebiche-Senhadji, L. Mansouri, S. Tingry, P. Seta, M. Benamor, Facilitated Cd(II) transport across CTA polymer inclusion membrane using anion (Aliquat 336) and cation (DE2HPA) metal carriers, J. Membr. Sci. 310 (2008) 438–445.
[33] A. Yilmaz, G. Arslan, A. Tor, I. Akin, Selectively facilitated transport of Zn(II) through a novel polymer inclusion membrane containing Cyanex 272 as a carrier reagent, Desalination 277 (2011) 301–307.
[34] F. Garbassi, M. Morra, E. Occhiello, Polymer Surfaces from Physics to Technology, Wiley, New York, NY, 1994.
[35] S.-T. Hwang, K. Kammermeyer, Membranes in Separations, Techniques of Chemistry, vol. VI, Wiley-Interscience, New York, NY, 1975.
[36] A. Al-Hajry, A. Umar, Y.B. Hahn, D.H. Kim, Growth, properties and dye-sensitized solar cells—Applications of ZnO nanorods grown by low-temperature solution process, Superlat. Microstruct. 45 (2009) 529–534.
[37] A. Umar, M.M. Rahman, A. Alhajry, Y.B. Hahn, Highly-sensitive cholesterol biosensor based on well-crystallized flower-shaped ZnO nanostructures, Talanta 78 (2009) 284–289.
[38] O. Arous, F. Saad Saoud, H. Kerdjoudj, Cellulose triacetate properties and their effect on the thin films morphology and performance, IOP Conf. Series, Mater. Sci. Engineer. 12 (2010) 012001-1–012001-5.
[39] S. Balta, A. Sotto, P. Luis, L. Benea, B.V. Van der Bruggen, J. Kim, A new outlook on membrane enhancement with nanoparticles: The alternative of ZnO, J. Membr. Sci. 389 (2012) 155–161.
[40] S. Oh, T. Kang, H. Kim, J. Moon, S. Hong, J. Yi, Preparation of novel ceramic membranes modified by mesoporous silica with 3-aminopropyltriethoxysilane (APTES) and its application to Cu^{2+} separation in the aqueous phase, J. Membr. Sci. 301 (2007) 118–125.
[41] S. Elumalai, G. Muthuraman, Comparative study of liquid–liquid extraction and bulk liquid membrane for Rhodamine B, Inter. J. Eng. Innov. Technol. 3(2) (2013) 387–392.
[42] M.S. Alam, K. Inoe, Extraction of rhodium from other platinum group metals with Kelex 100 from chloride media containing tin, Hydrometallurgy 46 (1996) 373–382.
[43] J.A. Reyes-Aguilera, M.P. Gonzalez, R. Navarro, T.I. Saucedo, M. Avila-Rodriguez, Supported liquid membranes (SLM) for recovery of bismuth from aqueous solutions, J. Membrane Sci. 310 (2008) 13–19.
[44] F.J. Alguacil, A.G. Coedo, M.T. Dorado, A.M. Sastre, Uphill permeation of chromium (VI) using Cyanex 921 as ionophore across an immobilized liquid membrane, Hydrometallurgy (2001) 13–19.
[45] L. Mıtıche, S. Tıngry, P. Seta, A. Sahmoune, Facilitated transport of copper(II) across supported liquid membrane and polymeric plasticized membrane containing 3-phenyl-4-benzoylisoxazol-5-one as carrier, J. Membr. Sci. 325 (2008) 605–611.
[46] R. Navarro, I. Saucedo, A. Núñez, M. Ávila, E. Guibal, Cadmium extraction from hydrochloric acid solutions using Amberlite XAD-7 impregnated with Cyanex 921 (tri-octyl phosphine oxide), React. Funct. Polym. 68 (2008) 557–571.
[47] A. Salima, K. Ounissa, M. Lynda, B. Mohamed, Cationic dye (MB) removal using polymer inclusion membrane (PIMs), Procedia Eng. 33 (2012) 38–46.
[48] G. Muthuraman, T.T. Teng, Use of vegetable oil in supported liquid membrane for the transport of Rhodamine B, Desalination 249 (2009) 1062–1066.